

1
2 **Technical Note: On HALOE stratospheric water vapor variations and trends at Boulder,**
3 **Colorado**

4 **by**

5 **Ellis Remsberg**

6 **Science Directorate**

7 **21 Langley Blvd., Mail Stop 401B**

8 **NASA Langley Research Center**

9 **Hampton, Virginia USA, 23681**

10 **(email: Ellis.E.Remsberg@nasa.gov)**

11 **Atmospheric Chemistry and Physics Journal**

12 **(July 2023)**

13 **Abstract.** This study compares time series of stratospheric water vapor (SWV) data at 30 hPa
14 and 50 hPa from 1993 to 2005, based on sets of Halogen Occultation Experiment (HALOE)
15 profiles above the Boulder, CO (40°N, 255°E) region and on local frost-point hygrometer (FPH)
16 measurements. Their differing trends herein agree with most of the previously published
17 findings. FPH trends are presumed to be accurate within their data uncertainties, and there are
18 no known measurement biases affecting the HALOE trends. However, the seasonal sampling
19 from HALOE is deficient at 40°N from 2001 to 2005, especially during late winter and
20 springtime, when HALOE SWV time series at 55°N clearly show a springtime maximum. This
21 study finds that the SWV trends from HALOE and FPH nearly agree within uncertainties at 30
22 hPa for the more limited time span of 1993 to 2002. Yet, HALOE SWV at 50 hPa has
23 significant and perhaps uncertain corrections for interfering aerosols from 1992 to 1994.
24 Northern hemisphere time series and daily SWV plots near 30 hPa from the Limb Infrared
25 Monitor of the Stratosphere (LIMS) experiment indicate that there is transport of filaments of
26 high SWV from polar to middle latitudes during dynamically active, winter and springtime
27 periods. Although FPH measurements sense SWV variations at all scales, the HALOE time
28 series do not resolve smaller-scale structures because its time series data are based on an average
29 of four or more occultations within a finite latitude/longitude sector. It is concluded that the
30 variations and trends of HALOE SWV are reasonable at 40°N and 30 hPa from 1993 to 2002 and
31 in accord with the spatial scales of its measurements and sampling frequencies.

32

33 **1. Background and Objective**

34 There have been numerous studies of long-term changes of stratospheric water vapor (SWV)
35 mixing ratios (e.g., Konopka, et al., 2022; Hegglin et al., 2014; Hurst et al., 2011). SWV trends
36 in the lowermost stratosphere are affected mainly by non-zonal variations of the cold-point
37 temperature (CPT) at the tropical tropopause, followed by transport of the associated relatively
38 dry, entry-level air. Hegglin et al. (2014) also report on the roles of the oxidation of methane to
39 water vapor in the middle and upper stratosphere and of changes in the Brewer/Dobson
40 circulation (BDC) on water vapor trends throughout the stratosphere. One remaining puzzle is
41 that the SWV trends from frost-point hygrometer (FPH) measurements above Boulder, CO, are
42 more positive (or less negative) than zonal average and Boulder region analyses of SWV from
43 the Halogen Occultation Experiment (HALOE) (Scherer et al., 2008). Lossow et al. (2018)
44 reported that those differences increase with altitude, and they cautioned that trends over Boulder
45 may not be representative of zonal-mean values some years. Konopka et al. (2022) found from
46 reanalysis data that there is a moistening above the Boulder region during late boreal winter and
47 spring.

48

49 The present study reconsiders in Section 2 the HALOE SWV trends and variations near Boulder
50 for 1993 through 2005 and compares them in Section 3 with those from the Boulder FPH
51 measurements that are assumed to be accurate. The focus is on the trend differences at 30 hPa,
52 where Lossow et al. (2018) found that they were largest. Section 4 reports on the SWV trend
53 differences for the same years at 50 hPa, or where there may be biases in HALOE SWV from its
54 corrections for interfering aerosols. Section 5 shows a time series of northern hemisphere SWV
55 near 30 hPa from the Nimbus 7 Limb Infrared Monitor of the Stratosphere (LIMS) dataset of
56 1978-1979. Daily plots of LIMS geopotential height (GPH) and SWV show the effects of
57 meridional transport of SWV to 40°N during a dynamically active period in February 1979.
58 That example provides evidence of a late winter to spring moistening in the Boulder region.
59 There are also instances of elevated SWV in the HALOE time series at subpolar latitudes at that
60 time of year. Section 6 concludes that the HALOE SWV variations and trends at 40°N are
61 understandable compared with those from FPH, given the spatial scales of their measurements,

62 the reduction in sampling by HALOE after 2001, and possible HALOE SWV biases from
63 interfering aerosols.

64

65 **2. Time series analyses of HALOE SWV near Boulder**

66 SWV time series from the HALOE dataset are analyzed by multiple linear regression (MLR)
67 techniques in the manner of Remsberg (2008) and Remsberg et al. (2018a). Although HALOE
68 began operations in October 1991, its SWV profiles are degraded in the lower stratosphere in
69 1991 through mid-1992 because of solar tracking anomalies in the presence of the very large
70 extinction effects from Pinatubo aerosols. Figure 1a shows HALOE time series data from late
71 1991 through 2005 for the Boulder sector.

72

73 The Boulder region HALOE SWV points of Fig. 1a are for 30 hPa and are based on averages of
74 profiles within the latitude range of $40\pm 4^\circ\text{N}$ and the longitude range of $255\pm 35^\circ\text{E}$, since HALOE
75 seldom measured profiles at the exact location of Boulder. A rather narrow latitude range was
76 chosen for this study because there is a significant latitudinal gradient in SWV near 40°N in both
77 fall and springtime. The finite longitude range of $\pm 35^\circ$ attains four or more profiles, most times,
78 from the SR or SS orbital crossings near Boulder, and it is sufficient for indicating low zonal
79 wavenumber effects on the SWV field. The data in Fig. 1a from January 1993 onward are fit
80 with an MLR model that corrects for effects of lag-1 autoregression (AR1) and accounts for
81 memory between adjacent data points (Tiao et al., 1990); its AR1 coefficient is 0.35. The MLR
82 model fit to the data of January 1993 through 2005 (solid curve) includes constant and linear
83 trend terms plus periodic annual (AO), semiannual (SAO) and QBO-like terms. The periodic
84 QBO-like term is approximated as a 28-mo cycle, based on a Fourier analysis of an initial time
85 series residual after accounting for the seasonal terms. The model also contains proxy terms for
86 El Nino/Southern Oscillation (ENSO) forcings and solar cycle flux forcings. Significant terms
87 are SAO, QBO-like, and ENSO proxy; the latter two terms account for differences from the fit of
88 the HALOE data in Fig. 1a versus that from a simple seasonal fitting. The dashed line in Fig. 1a
89 represents the sum of the constant term (4.84 ppmv) and a linear trend coefficient of -0.22 ± 0.04
90 ppmv/decade, having a confidence interval (CI) of 95% or a trend of $-4.5\pm 0.6(2\sigma)$ %/decade.

91 The SWV trend from Fig. 1a agrees closely with previous trends from HALOE data near 30 hPa
92 in the latitude range of 35°N to 45°N (Davis et al., 2016; Lossow et al., 2018).

93

94 All MLR term coefficients are reasonably accurate, if the seasonal sampling is good. However,
95 from 2001 through 2005 there are few to no sunrise (SR) or sunset (SS) samples in Fig. 1a from
96 late winter through springtime. That sampling deficit became longer because HALOE was
97 turned off a bit earlier prior to a UARS yaw maneuver and then turned on later following the yaw
98 event starting in 2001, to conserve power on the UARS spacecraft. While that change in
99 operating procedure accounts for the lack of HALOE measurements near 40°N during late winter
100 and springtime, the HALOE sampling frequency remains as earlier for lower and higher latitude
101 zones. As an example, HALOE SWV for the longitude sector of Boulder but at the higher
102 latitude zone of 55±10°N is in Figure 1b and shows that the seasonal sampling occurs more
103 regularly compared to that at 40°N in Fig. 1a. Northern hemisphere SWV attains its annual
104 maximum in late winter or early springtime, according to the MLR modeling of HALOE SWV at
105 55°N (Fig. 1b). Note that HALOE SWV at 55°N also has rather high values in early 2002 or
106 following stratospheric warming events in the winter of 2001-2002 (Charlton and Polvani, 2007).
107 There may have been transport of higher SWV values to 40°N that HALOE did not observe.

108

109 Separate MLR analyses of the SS and then the SR data points of Fig. 1a from 1993 to 2005 (not
110 shown) yield trends that are significantly more negative for SS (-0.30 ppmv/decade) than for SR
111 (-0.17 ppmv/decade). The HALOE SWV trends at 40°N for the time segment from 2001 to 2005
112 differ because of the timing of and/or lack of their late winter and springtime values. Even so, it
113 is expected that there ought to be decreasing SWV values at 40°N during those years in response
114 to the decrease in SWV in the tropical lower stratosphere in early 2001, as noted by Randel et al.
115 (2006), Scherer et al. (2008), Hegglin et al. (2014), and Konopka et al. (2022). They reported
116 that there was a slight delay for a decrease of SWV at 40°N because of the slow ascent of the dry
117 tropical air plus the subsequent meridional transport and mixing of that air to middle latitudes.

118

119 Scherer et al. (2008) noted that it is perhaps more appropriate to apply two, piecewise linear
120 trend terms for the MLR modeling of the HALOE SWV data in Fig. 1a, where there is a break
121 point in 2002. Thus, Figure 1c shows a separate trend analysis of HALOE SWV for the Boulder
122 sector at 40°N, but only for 1993 to 2002; its average SWV value is 4.62 ppmv and its shorter
123 trend term is no longer negative but positive at 0.22 ± 0.04 ppmv/decade (or $4.7 \pm 0.7(2\sigma)$
124 %/decade). Finally, Figure 2 is the residual (data minus MLR model curve) for the fit in Fig. 1a,
125 and its variations about the mean are of order ± 0.3 ppmv. An important test of the adequacy of
126 the set of terms in its MLR model is whether any structure remains in the residual. No periodic
127 structure is apparent in Fig. 2, although there are clear seasonal gaps in the data series after 2001.

128

129 **3. Time series of FPH measurements of SWV**

130 Figure 3a is the SWV time series at 30 hPa from the FPH data at Boulder and for 1993-2005 for
131 comparison with Fig. 1a. Individual FPH profiles were interpolated vertically to obtain SWV
132 values at the 30-hPa level, and the FPH time series points are also spaced irregularly. SAO,
133 QBO, ENSO, and Linear terms from the MLR model of Fig. 3a have a significance of better than
134 90%. The constant term is 4.70 ppmv, which is a bit less than that from the HALOE series (4.84
135 ppmv) but within the estimated systematic uncertainties for both measurements. The FPH trend
136 for 1993-2005 is positive or $+0.17 \pm 0.07$ ppmv/decade (or $+3.6 \pm 1.5(2\sigma)$ %/decade), as compared
137 to the negative trend from HALOE ($-4.5 \pm 0.6(2\sigma)$ %/decade). There is also a change in trend
138 around 2002 in the FPH data of Fig. 3a, although it is not so apparent because of the rather large
139 scatter of the FPH points. Figure 3b shows the corresponding FPH MLR analysis for 1993 to
140 2002, which yields an average SWV of 4.62 ppmv and agrees with the average HALOE value
141 from Fig. 1c. The FPH trend for 1993 to 2002 is $+0.32 \pm 0.6$ ppmv/decade (or $+6.9 \pm 1.2$
142 %/decade), which is more positive than that of HALOE ($+4.7 \pm 0.7$ %/decade) but only slightly
143 outside the overlapping envelope (e.g., +5.7 versus +5.4 %/decade) from their mutual trend
144 uncertainties.

145

146 Figure 4 shows the residual (FPH minus MLR) for the time series data of Fig. 3a, where the FPH
147 points exhibit more scatter compared with the HALOE residual in Fig. 2. Data points of the FPH

148 record are assumed to be valid and accurate to $<6\%$ or about ± 0.3 ppmv, according to the
149 extensive studies of Hall et al. (2016). The rather large scatter in Fig. 4 exceeds that uncertainty.
150 Local FPH measurements are sensitive to SWV variations across all spatial scales. Note that the
151 structure in the FPH residual of Fig. 4 is aperiodic and presumably due to small-scale
152 atmospheric variations in some instances. Accordingly, it is difficult for the MLR modeling to
153 fit all the real structure in the FPH data, and its linear trend term is not highly significant.
154 Conversely, each individual HALOE profile gives an SWV value that is an average across its
155 tangent view path (~ 300 km) and with a vertical resolution of no better than two kilometers. The
156 HALOE time series points are also based on sector averages of four or more profiles. Thus,
157 HALOE does not resolve SWV variations at small to intermediate scales.

158
159 There are high FPH SWV values in Fig. 3 on 22 May (5.8 ppmv) and on 26 June 1996 (5.5
160 ppmv), possibly due to elevated SWV in filaments of polar vortex air that were transported to
161 and remained isolated above the location of Boulder for days to weeks (e.g., Manney et al.,
162 2022). A search of individual profiles from HALOE reveals SWV values of order 6.5 ppmv at
163 60°N , 270°E in mid-March 1996. Temperature at that higher latitude location is only 200 K and
164 methane is only 0.4 ppmv, both of which are characteristic of winter vortex air. HALOE also
165 found a small region of high SWV (~ 5.8 ppmv) and low methane in several soundings near
166 44°N , 170°E on 12 May 1996. In another instance, FPH has high SWV on 12 April 2000 (5.9
167 ppmv). HALOE SWV approached 7.0 ppmv near 60°N , 270°E about a month earlier on 18
168 March 2000; there are also several HALOE values greater than 5.0 ppmv at 40°N on 20 April
169 2000. An example of a source of the elevated SWV is considered in Section 5.

170

171 **4. Uncertainties for the HALOE SWV trends**

172 Gordley et al. (2009) reported that there are no indications of an instrument bias for the HALOE
173 SWV trends. However, HALOE SWV profiles can be affected by residual effects from cloud
174 tops and subvisible cirrus, as shown for HALOE ozone (Bhatt et al., 1999). As a result, HALOE
175 SWV trends at pressure levels of 100 hPa and even 70 hPa may not be accurate. Harries et al.
176 (1996) also reported that HALOE SWV profiles are uncertain at 40 hPa by 8% in 1992 because

177 of interfering aerosols, and Hervig et al. (1995) showed that there are significant corrections for
178 Pinatubo aerosols at 36°N in mid-1992 for the retrieval of HALOE SWV at 30 hPa and,
179 especially at 50 hPa.

180
181 Figure 5 shows HALOE SWV time series points at 50 hPa, where there is a decrease of SWV
182 starting in mid-2001. Its trend from December 1992 to 2005 is negative or -6.6 ± 0.9 %/decade.
183 Yet, the MLR trend is positive ($+3.7 \pm 1.4$ %/decade) for the shorter period of December 1992 to
184 mid-2001 or just prior to the abrupt decrease. Its model SAO, AO, QBO, and ENSO terms are
185 significant, and its mean value is 4.28 ppmv. A secondary trend for the somewhat shorter (and
186 later) period of January 1994 to mid-2001 is already negative (-4.2 ± 1.2 %/decade) and nearer to
187 that of the full period of December 1992 to 2005. It may be that the aerosol correction model has
188 a bias error that affects retrieved SWV from December 1992 to January 1994.

189
190 Aerosol extinction profiles are determined from wavelengths of the HALOE gas filter correlation
191 channels of HF, HCl, CH₄, and NO (Hervig et al., 1995). Then, corrections for the HALOE
192 radiometer channels (H₂O, NO₂, and O₃) are a modeled extrapolation with wavelength from the
193 NO channel aerosol profile at 5.26 micrometers. Example comparisons of retrieved HALOE
194 SWV versus correlative measurements indicate that the modeled corrections are qualitatively
195 correct in 1992 (Hervig et al., 1996). Nevertheless, the model for aerosol absorption versus
196 wavelength assumes a size distribution shape and an aqueous sulfuric acid composition (i.e.,
197 refractive index) that is constant with altitude and over time. Effectively, the aerosol corrections
198 represent a change in aerosol number density only. That correction model was employed for the
199 decay of the Pinatubo aerosol layer, as well as for near background aerosols. Hervig et al. (1995)
200 estimated the effect of those biases on HALOE SWV at 50 hPa is ± 0.8 ppmv for a profile at
201 36°N in September 1992, or when the aerosol extinction was $5 \times 10^{-4} \text{ km}^{-1}$ or close to the
202 beginning date of December 1992 in the MLR analysis of Fig. 5. The HALOE data show that
203 aerosol extinction and its effects on SWV had declined by about a factor of five by January 1994.

204

205 Figure 6 is the corresponding FPH time series at 50 hPa. It shows no clear change in 2001,
206 largely a consequence of the scatter of its data points. Its mean SWV value from late 1992 to
207 mid-2001 is 4.21 ppmv, but its trend is $+10.8 \pm 1.7$ %/decade or much larger than from HALOE.
208 Still, it is noted that the FPH trends are variable with time because of the significant scatter of the
209 points in its time series. Nevertheless, the HALOE versus FPH trend differences at 50 hPa are
210 qualitatively like those obtained by Scherer et al. (2008, their Fig. 7).

211
212 HALOE measurements at 30 hPa are affected by a lower aerosol extinction of $2 \times 10^{-4} \text{ km}^{-1}$
213 from September to December 1992, and its SWV values are uncertain by only ± 0.2 ppmv. Note
214 that the SWV trend at 30 hPa agreed better with that from FPH (HALOE from Fig. 1c is $+4.7$
215 %/decade and FPH from Fig. 3b is $+6.9$ %/decade). By January 1994 the aerosol extinction
216 values at 30 hPa declined by nearly a factor of ten, and HALOE SWV is nearly unaffected by
217 aerosol corrections thereafter.

218
219 HALOE SWV trends should be most accurate in the absence of aerosols. As a check on that
220 likelihood, Figure 7 shows the corresponding fit of the HALOE SWV time series from 1993 to
221 2002 at 20 hPa, or just above the top of the volcanic aerosol layer. SWV has a positive vertical
222 mixing ratio gradient with altitude, due to the oxidation of methane to SWV in the middle
223 stratosphere, and average SWV at 20 hPa is 4.74 ppmv or a bit higher than that at 30 hPa (4.62
224 ppmv). A combined AO/SAO maximum shows clearly in Fig. 7, where the AO amplitude is
225 twice that of the SAO and the AO and SAO phase maxima occur on 19 February and 9 April,
226 respectively. Those seasonal cycles confirm the late winter/early spring moistening found in
227 reanalysis data at 40°N by Konopka et al. (2022).

228
229 The HALOE SWV trend at 20 hPa for 1993-2002 is $+6.9 \pm 0.9$ (2σ) %/decade, which agrees with
230 that at 30 hPa from FPH ($+6.9 \pm 1.2$ %/decade). (There are too few FPH data at 20 hPa for a
231 direct trend comparison with HALOE.) Yet, the HALOE trend at 20 hPa is significantly more
232 positive than its trend at 30 hPa ($+4.7 \pm 0.7$ %/decade). Remsberg (2015, Table 1) reported
233 positive trends for HALOE methane in the tropical middle stratosphere of order 10%/decade, a

234 small fraction (certainly less than half) of which may have undergone an oxidization to SWV and
235 subsequent transport to 40°N. The increase of 2.2 %/decade for the HALOE SWV trend from 30
236 to 20 hPa could be due to that process alone. Thus, it is inferred that the HALOE aerosol
237 corrections at 30 hPa are small and quite reasonable over time, too.

238

239 **5. Source for the springtime moistening at 40°N**

240 Hegglin et al. (2014) and Remsberg (2015) showed that both methane and water vapor from
241 limb-viewing satellite datasets (SPARC, 2017) are good indicators of seasonal variations of the
242 BDC in the stratosphere. They reported on a hemispheric asymmetry for the net circulation,
243 where the BDC in the northern hemisphere (NH) is stronger and its methane and relative SWV
244 trends are more positive than in the southern hemisphere. The strength of the NH BDC is
245 enhanced in winter, primarily due to effects of forcings from planetary waves. There is chemical
246 conversion of methane to water vapor in the middle and upper stratosphere followed by descent
247 of that relatively moist air to the lower stratosphere in the region of the polar vortex.

248

249 Seasonal SWV data from the LIMS experiment illustrate the above process for 1978-1979.
250 Figure 8 (from Remsberg et al., 2018b, their Fig. 14) displays a seasonal increase in SWV within
251 the NH on the 550 K potential temperature surface (near 30 hPa) in terms of its area diagnostic
252 versus equivalent latitude, which is a vortex-centered display of SWV along potential vorticity
253 contours. Fig. 8 indicates that enhanced values of water vapor descended to this surface in the
254 vortex region by early January and continued through March. Specifically, there was an
255 equatorward expansion of the average SWV value of 5.2 ppmv to the equivalent latitude of 40°N
256 during mid-February and from mid-March onward, as the high latitude air mixed with lower
257 latitude air. Note that the 550 K surface is well above the tropical tropopause, minimizing
258 effects due to any meridional exchanges of water vapor within the lowermost stratosphere.
259 Similar analyses of seasonal changes of ozone also show that there is further descent to lower
260 potential temperature levels during springtime and a similar transport and mixing of polar air to
261 lower latitudes at those levels (Curbelo et al., 2021).

262

263 Polar plots of LIMS Version 6 (V6) geopotential height (GPH) and SWV for 17 February 1979
264 are in Figures 9 and 10. They indicate the effects of meridional transport of polar air to middle
265 latitudes, in response to a high latitude, zonal wave-2 event. Fig. 9 shows high GPH (and
266 anticyclonic circulation) in the Aleutian and eastern Atlantic sectors and low GPH in the polar
267 vortex (cyclonic) that extends southward across North America. The associated higher values of
268 SWV in Fig. 10, though somewhat noisy, are characteristic of vortex air that also underwent a
269 southward transport. The vortex (region of highest SWV) is elongated and extends equatorward
270 around 90°E and 270°E. There is also a filament of high SWV (>5.5 ppmv) at the latitude of
271 Boulder and across adjacent longitudes. The seasonal time series display of NH SWV in Fig. 8
272 shows that this is when the 5.2 ppmv contour extends to near 40°N equivalent latitude.

273

274 Figure 8 also indicates that there was an initial descent of polar air with higher values of SWV to
275 near the 31.6 hPa surface around 10 January. Then there was a more general expansion of
276 elevated SWV to the equivalent latitude of 40°N by the end of January (follow the 4.8 ppmv
277 contour in Fig. 8). Similar instances of meridional transport and mixing to North American
278 middle latitudes are a likely cause of the sporadic appearance of high SWV values during the
279 winter and early spring seasons of the FPH measurements in Fig. 3 and in the recent reanalysis
280 studies of Konopka et al. (2022) and of Wargan et al. (2023). However, the HALOE time series
281 points in Fig. 1 do not resolve such features so well because they are based on averages of four
282 or more profiles from within the rather large sector around Boulder.

283

284 HALOE SWV time series were also analyzed for occurrences of higher SWV in three separate
285 longitude sectors (North America, 255±35°E; Aleutian, 180±35°E; and European, 35±35°E)
286 from 1993 to 2002. There are several such instances at 40°N in the Boulder sector (Fig. 1), but
287 none in the Aleutian or European sectors (not shown). Conversely, Figure 11 shows that there
288 are several positive SWV anomalies within the higher latitude zone of 53±7°N in the European
289 sector but none in the Boulder or Aleutian sectors (not shown). SWV in Fig. 11 approaches 6.0
290 ppmv in four instances (on 22 April 1994, 14 April 1996, 7 March 2000, and 14-19 February
291 2001), and average SWV is 5.14 ppmv. All four instances are accompanied by low values of
292 methane, which is a tracer of the transport of polar air to lower latitudes. The instances in 2000

293 and 2001 also occurred just after temperatures in the upper stratosphere were of order 270 K or
294 like that for a sudden stratospheric warming (SSW) event. There was a rather extended area of
295 higher SWV over Europe, not merely a filament of vortex air, following those events.

296

297 **6. Summary and Conclusions**

298 Analyses of time series of HALOE and FPH SWV were conducted at 30 hPa and 50 hPa for the
299 Boulder region. Sampling frequencies for both sets of time series are of the order of a few days
300 to several weeks. The SWV trend in the Boulder region is positive from the FPH and negative
301 from the HALOE data from 1993 to 2005. It is assumed that the time series of FPH SWV
302 measurements are accurate, or to within their uncertainties of $<6\%$; the foregoing HALOE/FPH
303 trend differences appear significant. However, there are rather large gaps at 40°N during late
304 winter and spring in the HALOE time series after 2001, due to the limited power that was
305 available for HALOE operations. This makes it is more difficult to resolve the seasonal terms
306 and the trend term from HALOE data after 2001.

307

308 The HALOE SWV trend goes from positive to negative around 2002, and that change is a
309 delayed effect following the sharp decrease in tropical, lower stratospheric SWV that occurred
310 early in 2001. The FPH time series has a trend that is less positive after 2001, too, although that
311 change is not so obvious because of the larger scatter for its points. It is more appropriate to fit
312 two, piecewise linear trends to both the HALOE and FPH time series with a break point in 2002.
313 There are no known measurement biases that are affecting the HALOE trends. However, the
314 retrievals of HALOE SWV do have significant and uncertain corrections for interfering aerosol
315 extinction following the eruption of Pinatubo, particularly at 50 hPa, where the trends from
316 HALOE and FPH disagree. The analyzed HALOE trend ($+4.7 \pm 0.7 \%$ /decade) at 30 hPa agrees
317 more closely with that from FPH ($+6.9 \pm 1.2 \%$ /decade), or where the aerosol corrections are
318 relatively small after 1992.

319

320 The HALOE SWV time series at 20 hPa clearly shows a springtime maximum. Northern
321 hemisphere SWV time series from the Limb Infrared Monitor of the Stratosphere (LIMS)
322 experiment indicate a transport of higher SWV from polar to middle latitudes during late winter
323 and springtime. Daily surface maps of LIMS SWV reveal filamentary structure at the latitude of
324 40°N during and following dynamically active periods. Surface maps of GPH verify that there
325 was meridional transport of high SWV from the polar vortex to the latitude of 40°N at those
326 times. Whereas FPH measurements sense SWV variations at all scales, the HALOE time series
327 do not resolve intermediate to smaller scale structure because its data points are based on an
328 average of four or more occultation profiles within a finite latitude/longitude sector centered on
329 Boulder. It is concluded that the variations and trends of HALOE SWV are reasonably accurate
330 at 40°N and 30 hPa for 1993 to 2002 and in accord with the spatial scales of its measurements
331 and its sampling frequencies.

332

333 **Data Availability**

334 The LIMS V6 Level 3 product and the HALOE V19 profiles are at the NASA EARTHDATA
335 site of EOSDIS and its Website as:

336 https://disc.gsfc.nasa.gov/datacollection/LIMSN7L3_006.html, and as

337 https://disc.gsfc.nasa.gov/datacollection/UARHA2FN_019.html, respectively.

338 Frost point hygrometer (Lev) data were downloaded from the NOAA website:

339 https://gml.noaa.gov/aftp/data/ozwv/WaterVapor/Boulder_New/.

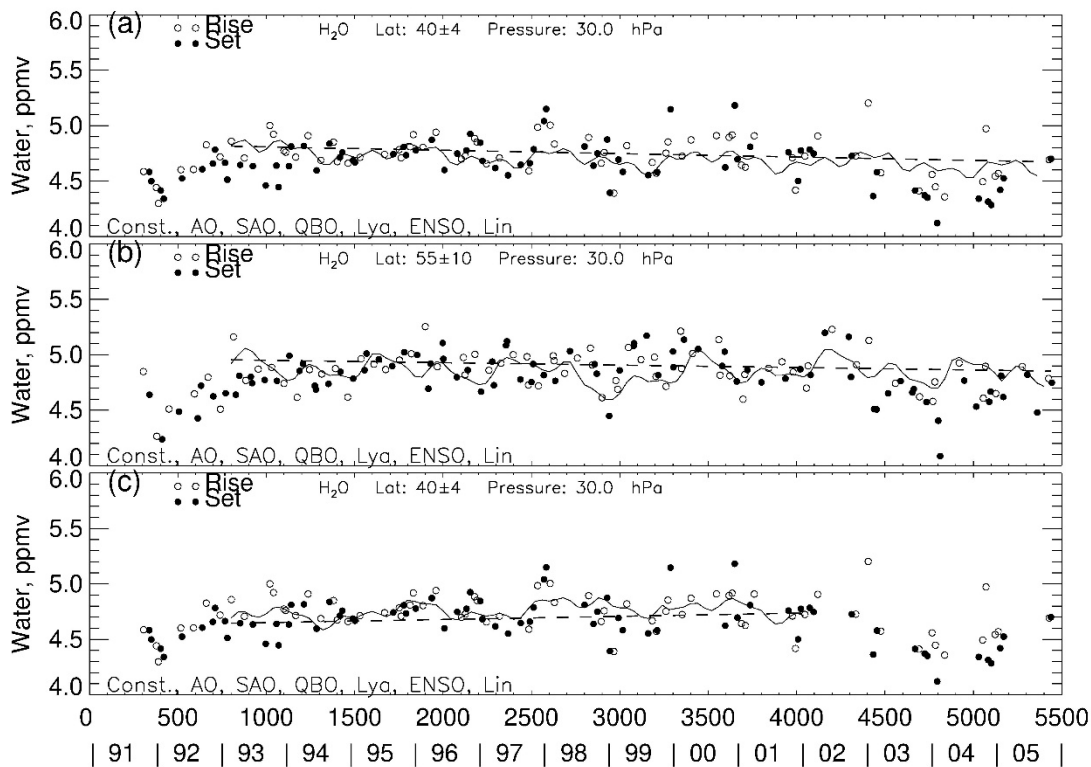
340

341 *Competing interests:* The author declares no competing interests.

342

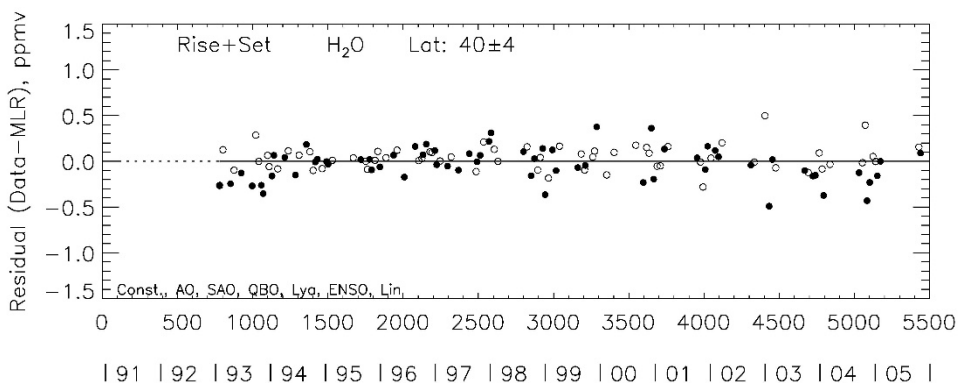
343 *Acknowledgements.* Author EER thanks V. Lynn Harvey for generating the plot in Figure 8 that
344 appeared originally in Remsberg et al. (2018b). EER also appreciates comments by Mark Hervig
345 on a draft of the manuscript. EER carried out this work while serving as a Distinguished
346 Research Associate of the Science Directorate at NASA Langley.

347



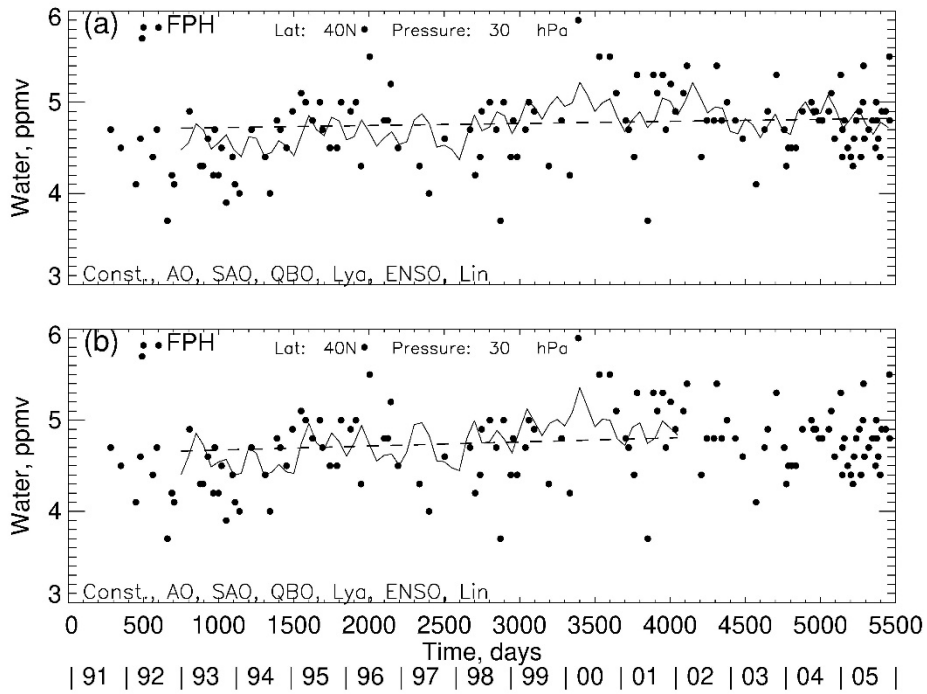
349
 350 Figure 1—MLR fit to a HALOE SWV time series; (a) Boulder sector, 40°N, 1993-2005, (b) at
 351 55°N, and (c) 40°N, 1993-2002. The fit of all the MLR terms is the oscillating curve; the linear
 352 trend term is the straight dashed line. Time by year or in days on abscissa begins Jan. 1, 1991.

353



354
 355 Figure 2—Residual from MLR model fit to HALOE time series data of Fig. 1(a).

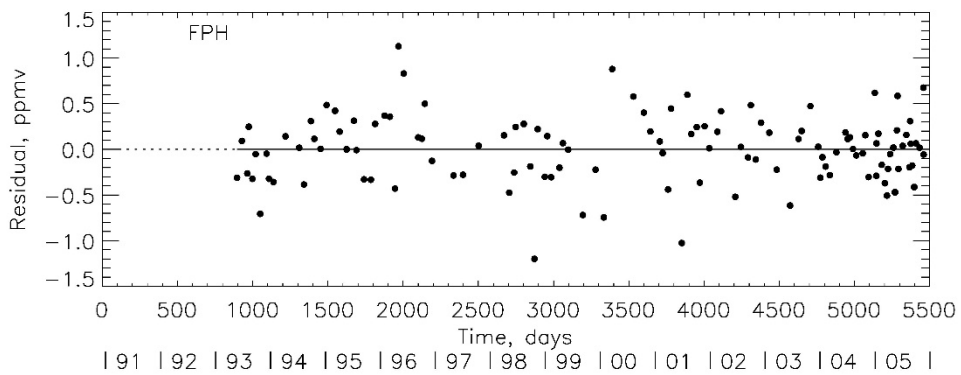
356



358

359 Figure 3—Time series of FPH data and MLR fit to them for comparison with Fig. 1; (a) 1993-
 360 2005, (b) 1993-2002.

361



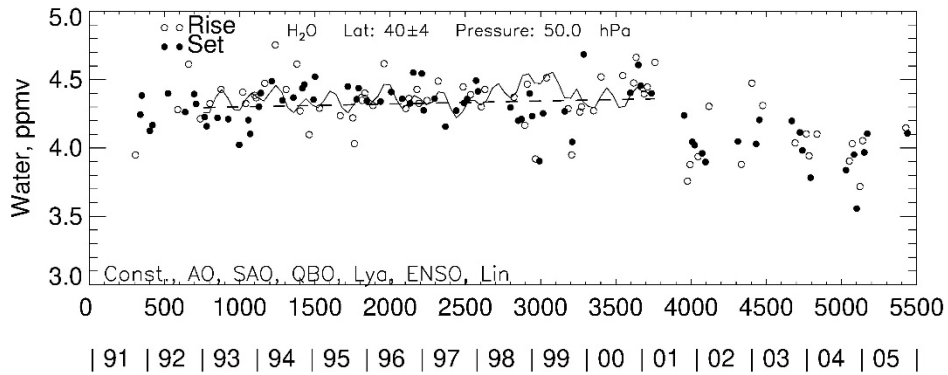
362

363 Figure 4—Time series residual for the MLR fit to the FPH data of Fig. 3(a).

364

365

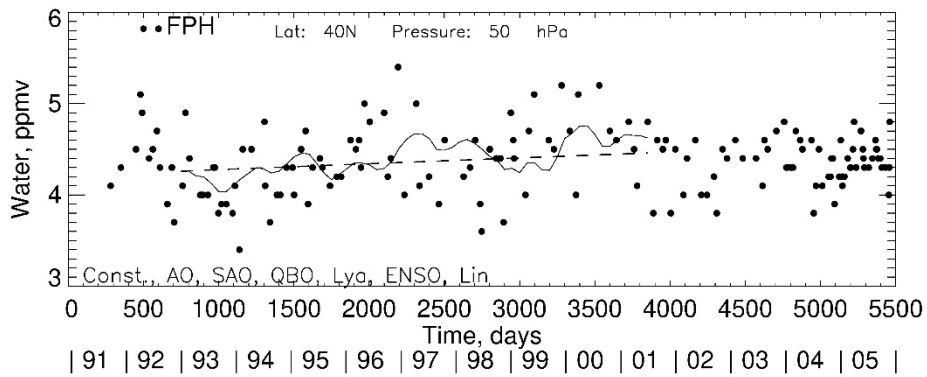
366



367

368 Figure 5—HALOE time series data at 50 hPa and MLR fit to them for 1993 to 2002.

369



370

371 Figure 6—As in Fig. 5, but for FPH data.

372

373

374

375

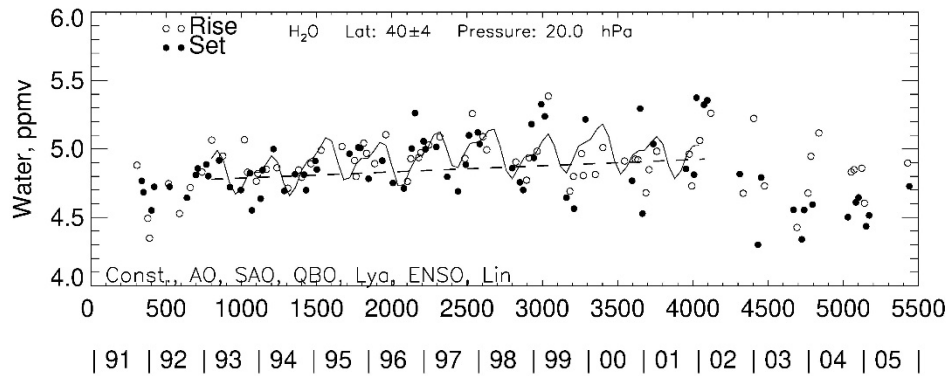
376

377

378

379

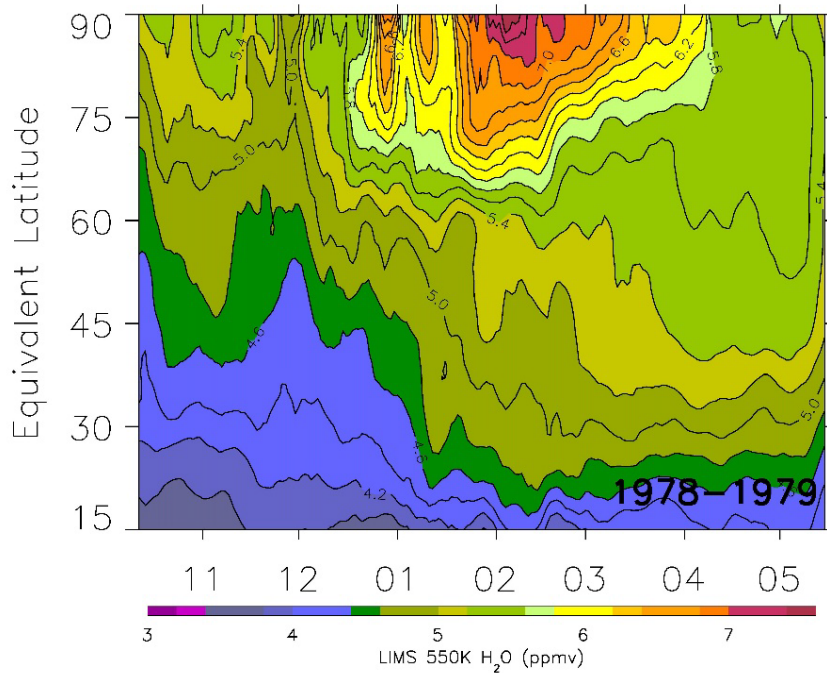
380



381

382 Figure 7—HALOE time series data at 20 hPa and MLR fit to them for 1993 to 2002.

383

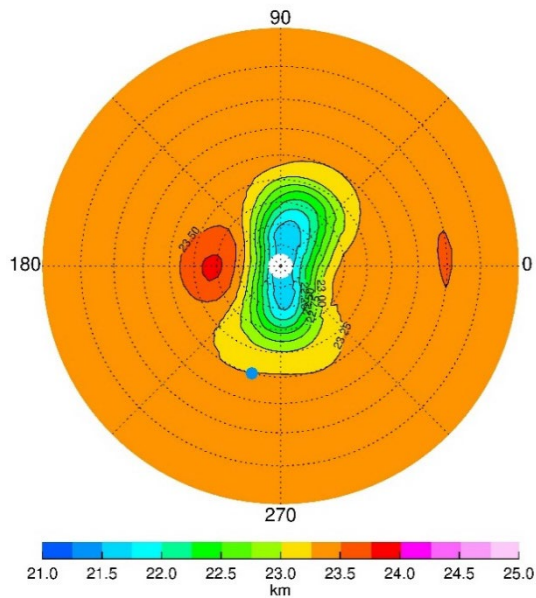


384

385 Figure 8—Time series of LIMS water vapor vs. equivalent latitude at 550 K and with smoothing
386 over 7 days. Contour interval is 0.2 ppmv. Tic marks along the abscissa denote the middle of
387 each month.

388

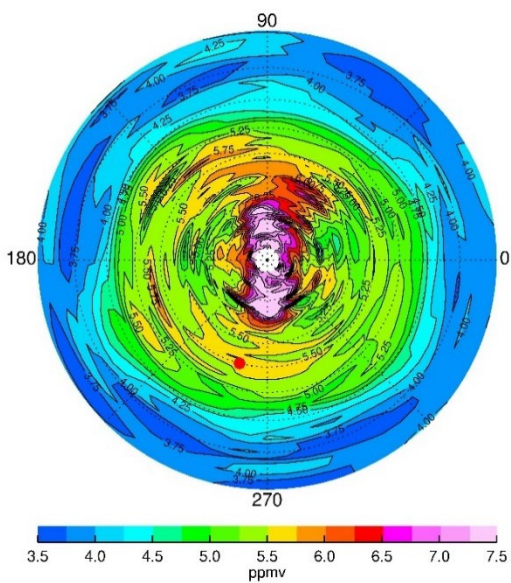
389



390

391 Figure 9—NH plot on the 31.6-hPa surface for 17 February 1979 of LIMS geopotential height
392 (GPH). Contour increment for GPH is 0.25 gpkm, and dashed circles are at every 10° of
393 latitude. Blue dot is location of Boulder, CO (40°N, 255°E).

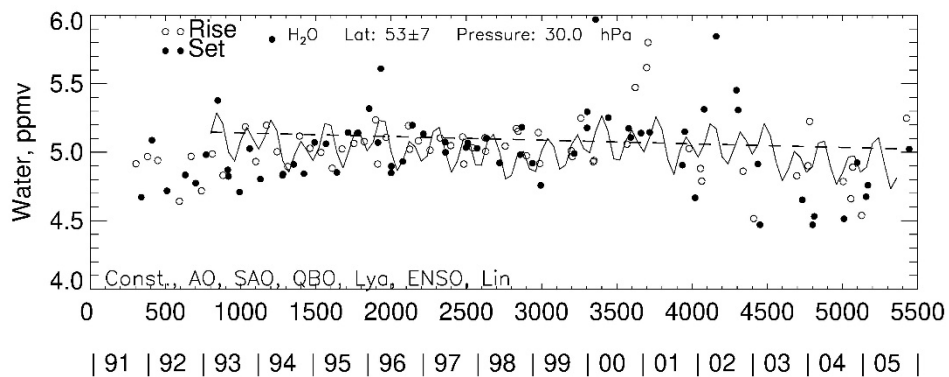
394



395

396 Figure 10—As in Fig. 9, but for LIMS SWV on 17 February. Contour interval (CI) is 0.25
397 ppmv. Red dot is location of Boulder.

398



399

400 Figure 11—As in Fig. 1(a), but for a European sector, centered at 53°N, 35°E.

401

402

403 **References**

404 Bhatt, P. P., Remsberg, E. E., Gordley, L. L., McInerney, J. M., Brackett, V. G., and Russell III,
405 J. M.: An evaluation of the quality of Halogen Occultation Experiment ozone profiles in the
406 lower stratosphere, *J. Geophys. Res.*, 104, <https://doi.org/10.1029/1999JD900058>, 1999.

407

408 Charlton, A. J., and Polvani, L. M.: A New Look at Stratospheric Sudden Warmings. Part I:
409 Climatology and Modeling Benchmarks, *J. Climate*, 20, <https://doi.org/10.1175/JCLI3996.1>,
410 2007.

411

412 Curbelo, J., Chen, G., & Mechoso, C. R.: Lagrangian analysis of the northern stratospheric polar
413 vortex split in April 2020. *Geophys. Res. Lett.*, 48, e2021GL093874.

414 <https://doi.org/10.1029/2021GL093874>, 2021.

415

416 Davis, S. M., Rosenlof, K. H., Hassler, B., Hurst, D. F., Read, W. G., Vömel, H., Selkirk, H.,
417 Fujiwara, M., and Damadeo, R.: The stratospheric water and ozone satellite homogenized
418 (SWOOSH) database: a long-term database for climate studies, *Earth Syst. Sci. Data*, 8, 461-490,
419 www.earth-syst-sci-data.net/8/461/2016/doi:10.5194/essd-8-461-2016, 2016.

420

421 Gordley, L. L., Thompson, E., McHugh, M., Remsberg, E., Russell III, J., and Magill, B.:
422 Accuracy of atmospheric trends inferred from the Halogen Occultation Experiment data, *J. Appl.*
423 *Remote Sensing*, 3, <https://doi.org/10.1117/1.3131722>, 2009.

424

425 Hall, E. G., Jordan, A. F., Hurst, D. F., Oltmans, S. J., Vömel, H., Kühnreich, B., and Ebert, V.:
426 Advancements, measurement uncertainties, and recent comparisons of the NOAA frost point
427 hygrometer, *Atmos. Meas. Tech.*, 9, <https://doi.org/10.5194/amt-9-4295-2016>, 2016.

428

429 Harries, J. E., Russell III, J. M., Tuck, A. F., Gordley, L. L., Purcell, P., Stone, K., Bevilacqua,
430 R. M., Gunson, M., Nedoluha, G., and Traub, W. A.: Validation of measurements of water vapor

431 from the Halogen Occultation Experiment (HALOE), *J. Geophys. Res.*, 101,
432 <https://doi.org/10.1029/95JD02933C>, 1996.

433

434 Hegglin, M. I., Plummer, D. A., Shepherd, T. G., Scinocca, J. F., Anderson, J., Froidevaux, L.,
435 Funke, B., Hurst, D., Rozanov, A., Urban, J., von Clarmann, T., Walker, K. A., Wang, H. J.,
436 Tegtmeier, S., and Weigel, K.: Vertical structure of stratospheric water vapour trends derived
437 from merged satellite data, *Nature Geoscience*, 7(10), 768–776.
438 <https://doi.org/10.1038/NGEO2236>, 2014.

439

440 Hervig, M. E., Russell III, J. M., Gordley, L. L., Park, J. H., Drayson, S. R., and Deshler, T.:
441 Validation of aerosol measurements from the Halogen Occultation Experiment, *J. Geophys. Res.*,
442 101, <https://doi.org/10.1029/95JD02464>, 1996.

443

444 Hervig, M. E., Russell III, J. M., Gordley, L. L., Daniels, J., Drayson, S. R., Park, J. H.: Aerosol
445 effects and corrections in the Halogen Occultation Experiment, *J. Geophys. Res.*, 100,
446 <https://doi.org/10.1029/94JD02143>, 1995.

447

448 Hurst, D. F., Oltmans, S. J., Vömel, H., Rosenlof, K. H., Davis, S. M., Ray, E. A., Hall, E. G.,
449 and Jordan, A. F.: Stratospheric water vapor trends over Boulder, Colorado: Analysis of the 30
450 year Boulder record, *J. Geophys. Res.*, 116, <https://doi.org/10.1029/2010JD015065>, 2011.

451

452 Konopka, P., Tao, M., Ploeger, F., Hurst, D. F., Santee, M. L., Wright, J. S., and Riese, M.:
453 Stratospheric moistening after 2000, *Geophysical Research Letters*, 49, e2021GL097609.
454 <https://doi.org/10.1029/2021GL097609>, 2022.

455

456 Lossow, S., Hurst, D. F., Rosenlof, K. H., Stiller, G. P., von Clarmann, T., Brinkop, S., Dameris,
457 M., Jöckel, P., Kinnison, D. E., Pliening, J., Plummer, D. A., Ploeger, F., Read, W. G.,
458 Remsberg, E. E., Russell III, J. M., and Tao, M.: Trend differences in lower stratospheric water

459 vapour between Boulder and the zonal mean and their role in understanding fundamental
460 observational discrepancies, *Atmos. Chem. Phys.*, 18, 8331-8351, [https://doi.org/10.5194/acp-](https://doi.org/10.5194/acp-18-8331-2018)
461 [18-8331-2018](https://doi.org/10.5194/acp-18-8331-2018), 2018.

462

463 Manney, G. L., Millan, L. F., Santee, M. L., Wargan, K., Lambert, A., Neu, J. L., Werner, F.,
464 Lawrence, Z. D., Schwartz, M. J., Livesey, N. J., and Read, W. G.: Signatures of Anomalous
465 Transport in the 2019/2020 Arctic Stratospheric Polar Vortex, *J. Geophys. Res. Atmospheres*,
466 127, e2022JD037407, <https://doi.org/10.1029/2022JD037407>, 2022.

467

468 Randel, W. J., Wu, F., Vömel, H., Nedoluha, G. E., and Forster, P.: Decreases in stratospheric
469 water vapor after 2001: Links to changes in the tropical tropopause and the Brewer-Dobson
470 circulation, *J. Geophys. Res. Atmospheres*, 111, <https://doi.org/10.1029/2005JD006744>, 2006.

471

472 Remsberg, E.: Methane as a diagnostic tracer of changes in the Brewer-Dobson circulation of the
473 stratosphere, *Atmos. Chem. Phys.*, 15, 3739-3754, <https://doi.org/10.5194/acp-15-3739-2015>,
474 2015.

475

476 Remsberg, E. E.: On the response of Halogen Occultation Experiment (HALOE) stratospheric
477 ozone and temperature to the 11-yr solar cycle forcing, *J. Geophys. Res.-Atmospheres*, 113,
478 <https://doi.org/10.1029/2008JD010189>, 2008.

479

480 Remsberg, E., Damadeo, R., Natarajan, M., and Bhatt, P.: Observed responses of mesospheric
481 water vapor to solar cycle and dynamical forcings, *J. Geophys. Res.*, 123, 3830-3843,
482 <https://doi.org/10.1002/2017JD028029>, 2018a.

483

484 Remsberg, E., Natarajan, M., and Harvey, V. L.: On the consistency of HNO₃ and NO₂ in the
485 Aleutian High region from the Nimbus 7 LIMS Version 6 dataset, *Atmos. Meas. Tech.*, 11,
486 3611-3626, <https://doi.org/10.5194/amt-11-3611-2018>, 2018b.

487

488 Scherer, M., Vömel, H., Fueglistaler, S., Oltmans, S.J., and Staehelin, J.: Trends and variability
489 of midlatitude stratospheric water vapour deduced from the re-evaluated Boulder balloon series
490 and HALOE, *Atmos. Chem. Phys.*, 8, 1391–1402, www.atmos-chem-phys.net/8/1391/2008/,
491 2008.

492

493 *SPARC Report No. 8 of the SPARC Data Initiative: Assessment of stratospheric trace gas and*
494 *aerosol climatologies from satellite limb sounders*, Prepared by the SPARC Data Initiative Team
495 and edited by M. I. Hegglin and S. Tegtmeier, WCRP-5/2017, Geneva,
496 <https://doi.org/10.3929/ethz-a-010863911>, 2017.

497

498 Tiao, G. C., Reinsel, G. C., Xu, D., Pedrick, J. H., Zhu, X., Miller, A. J., DeLuisi, J. J., Mateer,
499 C. L., and Wuebbles, D. J.: Effects of autocorrelation and temporal sampling schemes on
500 estimates of trend and spatial correlation, *J. Geophys. Res.*, 95, 20507–20517,
501 <https://doi.org/10.1029/JD095iD12p20507>, 1990.

502

503 Wargan, K., Weir, B., Manney, G. L., Cohn, S. E., Knowland, K. E., Wales, P. A., and Livesey,
504 N. J.: M2-SCREAM: A stratospheric composition reanalysis of Aura MLS data with MERRA-2
505 transport. *Earth and Space Science*, 10, e2022EA002632.,
506 <https://doi.org/10.1029/2022EA002632>, 2023.

507